Journal of Materials Chemistry A

Accepted Manuscript

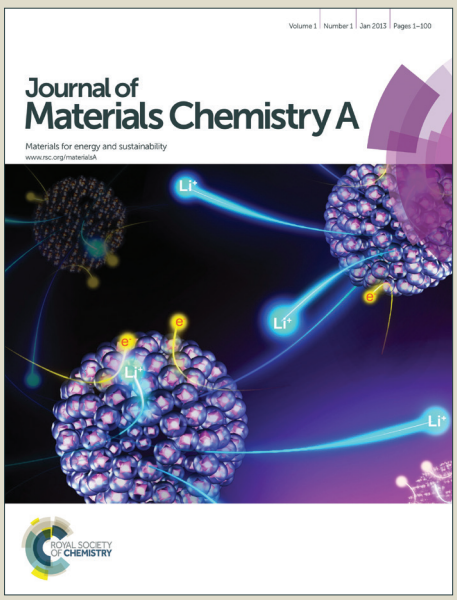

ROYAL SOCIETY OF CHEMISTRY

www.rsc.org/materialsA

Journal Name Journal of Materials Chemistry A Dynamic Article Links ►

Cite this: DOI: 10.1039/c0xx00000x

www.rsc.org/xxxxxx

ARTICLE TYPE

Facile preparation of MnO_2 doped Fe_2O_3 hollow nanofibers for low temperature SCR of NO with NH_3

Sihui Zhan,*[a] Mingying Qiu, *[a] Shanshan Yang[a], Dandan Zhu,[a] Hongbing Yu [a] and Yi Li*[b]

Received (in XXX, XXX) Xth XXXXXXXXX 20XX, Accepted Xth XXXXXXXXX 20XX

DOI: 10.1039/b000000x

Abstract: A series of MnO_2 doped Fe_2O_3 hollow nanofibers with different Mn/Fe molar ratios were successfully synthesized by the electrospinning method for the low temperature selective catalytic reduction (SCR) of NO with NH_3 in the presence of excess O_2. The SEM and TEM showed obvious hollow tubular structure of electrospun nanofibers. The hollow nanofibers with Mn/Fe molar ratio of 0.15 exhibited highest catalytic activity, nearly 100% of NO conversion from 150 to 300 °C, among the catalysts investigated. The TPR, XPS and in situ FTIR results revealed that Mn^{4+} was the main active species for SCR reaction and the addition of Mn species enhanced the surface concentration and acidity of Lewis acid sites.

1. Introduction

Nitrogen oxides (NOx) from industrial flue gas have been leading to more and more environmental problems including photochemical smog, acid rain and ozone depletion. [1-4] So far, selective catalytic reduction (SCR) of NO_x with NH_3 is the most effective technology for removing of NOx,[5-6] and commercial V_2O_5-WO_3/TiO_2 catalysts has been widely used for the removal of NOx from stationary sources.[7-11] However, there are some drawbacks of V_2O_5-WO_3/TiO_2 catalysts, such as high cost, the toxicity of vanadium species and narrow temperature window of 300-400 °C.[12] Thereby, it is necessary to develop novel low-temperature SCR catalysts, which can be set down at downstream of desulfurization scrubber or particulate control device, in order to avoid deactivation and save energy.[13,14]

Previous studies have showed that mixed transition metal oxides including Cu, Fe, Co, Mn, Ce, Cr, and Ni have the advantages of good low-temperature SCR activity and low cost. Among them, manganese and iron oxides are attracting much attention because of their high SCR activity at low temperature, low cost, and non-toxicity.[15-20] However, these Fe-base catalysts were prepared usually with the impregnation approach and were prone to be easily deactivated by SO_2 present in the treated flue gas. Therefore, the stability of catalytic activity, sulfur tolerance, and water resistance should be enhanced through formulation modification and structure adjustment.

In the past years, various methods have been used to synthesize nanoparticles including hydrothermal methods,[20-23] sol-gel,[24] and co-precipitation.[25] However, in catalytic processes, pore diffusion resistance is obvious for nanoparticles, which is hard to handle and usually causes many serious problems of high pressure drop in industrial application.[26] To overcome these disadvantages, electrospinning is applied for synthesizing hollow nanofibers or tubules, which have attracted much attention for their hierarchical tubules-within-a-tubule structure, as well as fibrous mat structure, large surface area and sufficient mechanical integrity. Just because of these advantages, the long hollow fibers could act as a micro-reactor and could be packed or constructed in the best form to fit the particular application in many fields, such as energy storage, semiconductor, gas sensor, and so on.[27-29] However, to the best of our knowledge, there is no report on using electrospun nanofibers as SCR catalyst to remove NOx with NH_3.

In this paper, manganese doped iron-based hollow nanofiber were successfully synthesized by electrospinning the corresponding precursor and calcination. The activities for the low temperature SCR of NO with NH_3 in the presence of excess O_2 at the relatively high space velocity of 50000 h^{-1} were investigated. The hollow nanofibers with Mn/Fe molar ratio of 0.15 exhibited an excellent NOx SCR performance of complete NO reduction at as low as 150 °C, which can be attributed to its relatively high surface area, high surface Mn^{4+} concentration, and the high concentration of Lewis acid sites, as well as, as characterized by BET, XPS, TPR, and in situ FTIR.

2. Experimental Section

2.1 Catalyst Preparation

All used chemicals were analytical grade. Citric acid, ferric citrate and manganese acetate were purchased from Sinopharm chemical reagent company without further purification.

In a typical process, 0.03 mol of citric acid and 0.01 mol of ferric citrate were dissolved into 50 mL deionized water with magnetic stirring for 3h, which is then filtered to remove insoluble contaminants to obtain a transparent solution A. Meanwhile, 0.001 mol manganese acetate was dissolved in 5 mL deionized water in order to obtain solution B. After being dissolved completely, solution B was poured into solution A with magnetic

stirring for 30 min at room temperature, then the mixed solution was aged at 60 °C for 24 h to 4-5 Pa·s.

In a typical electrospinning process, the spinnable sol was transferred into a plastic injector, and the sol was pressurized with a syringe pump (Cole-Parmer 74900-05, USA). The metallic needle was connected to a high-voltage supply (DW-P503-4ACCD, Tianjin, China), and a piece of stainless steel board was used to collect the gel fibers. All the experiments were conducted at room temperature, the applied voltage was 15 kV, the distance between the spinneret and the collector was 10 cm. Finally, the xerogel fibers were calcined at 400 °C for 4 h in air at a heating rate of 0.5 °C·min^{-1} to get the desired products. The hollow nanofibers were denoted as MnFe(x) ("x" represented the $MnOx/Fe_2O_3$ molar ratio; x = 0, 0.01, 0.05, 0.10, 0.15, 0.20). All the above catalysts were ground and sieved to 40-60 mesh for further measurements.

2.2. Catalyst Characterization

The morphology and structure of the fibers were observed by using a scanning electron microscope (SEM, Shimadzu SS-550) and a high-resolution transmission electron microscopy (HRTEM, Tecnai G2F20). The X-ray diffraction (XRD) patterns of samples were recorded via an X-ray diffractometer (Rigaku D/Max 2200PC) with a graphite monochrometer and CuKα radiation (λ=0.15418 nm) in the range of 20-80°. The voltage and current were 40 kV and 40 mA, respectively. The Fourier transform infrared spectroscopy (FTIR) spectra were recorded on a Nicolet 5DX-FTIR spectrometer using KBr pellet method in the range of 400-4000 cm^{-1}. N_2 adsorption-desorption data were obtained using a Quantachrom SI Micromeritics apparatus. X-ray photoelectron spectroscopy (XPS) spectra were collected on an ESCALAB 250 multi-technique X-ray photoelectron spectrometer (UK) using a monochromatic AlKα X-ray source (hν=1486.6 eV). All XPS spectra were recorded using an aperture slot of 300*700 microns, and survey spectras were recorded with pass energy of 160 eV, and high resolution spectra with a pass energy of 40 eV. Temperature-programmed reduction (H_2-TPR) experiments were conducted on a Micromeritics ChemiSorb 2720 using approximately 20 mg of samples. Samples were pretreated at 300 °C for 1 h in N_2 flow. The temperature was increased linearly from 50 to 1000 °C at 10 °C/min while H_2 consumption was recorded continuously. The in situ DRIFTS spectra were recorded with on an AVATAR 370 Fourier transform infrared spectrometer. Prior to each experiment, the sample was heated to 350 °C in He for 1h and then cooled to 150 °C. The spectra were recorded by accumulating 32 scans at a resolution of 4 cm^{-1}.

2.3. SCR Activity Measurements

The catalytic activities were evaluated using a bench-scale experimental system. In each test, hollow fibrous catalyst was loaded in a temperature controlled fixed-bed quartz flow reactor (i.d. 20 mm) containing 0.5 g of catalyst to control the reaction temperature. All individual flue gas components were precisely controlled by mass flow controllers (MFC), with a total flow rate of 300 mL·min^{-1} (refers to 1 atm and 298 K), which corresponded to a gas hourly space velocity (GHSV) of 50,000 h^{-1}. The typical composition of the initial reactant gas was: 500 ppm NO, 500 ppm NH_3, 5 vol % O_2, and balance N_2. The NO, NH_3, NO_2 and N_2O concentrations at both the inlet and outlet of the reactor were measured online by a FTIR spectrometer (Gasmet FTIR DX4000, Finland). The reaction system was kept for 1 h at each reaction temperature to reach a steady state before the analysis of the catalyst was performed. The NOx conversion as follows:

$$\text{NO conversion}\,(\%) = 100\% \times (1 - [\text{NOx}]_{out}/[\text{NOx}]_{in})$$

$$N_2\,\text{selectivity}\,(\%) = 100\% \times \{1 - ([NO_2]_{out} + 2[N_2O]_{out})/([\text{NOx}]_{in} + [NH_3]_{in} - [NH_3]_{out})\}$$

Where [NOx] = [NO] + [NO_2], and the subscripts "in" and "out" indicate the inlet concentration and outlet concentration at steady state, respectively.

3. Results and Discussion

3.1 Characteristics

To obtain structural information of the MnFe composite hollow nanofibers, XRD patterns were shown in Fig. 1. There were five diffraction peaks at 31.28, 35.08, 43.18, 56.58 and 62.88°, which belonged to magnetite Fe_2O_3 (PDF#19-0629). With increasing manganese content, the diffraction peak of Fe_2O_3 became lower and lower, indicating its composed nanoparticles became larger and larger.[30,31] However, no visible phase of Mn species could be observed, it may be due to the fact that MnOx is well incorporated into the matrix of Fe_2O_3 or that the Mn oxides were in a highly dispersed state or the crystallites formed were less than 5 nm beyond detection limitation. Furthermore, the full width at half-maximum (fwhm) of the peaks for MnFe(x=0.01-0.2) were lower than those for Fe_2O_3, indicating that the grain size of Fe_2O_3 on MnFe(x=0.01-0.2) was smaller than that on Fe_2O_3. This meant that the existence of MnOx could lower the crystallinity of Fe_2O_3 and thus enhance the dispersion of Fe_2O_3 on the catalyst surface.

The N_2 adsorption-desorption isotherms were shown in Fig 2, and data of pore size distribution, pore volume, and surface area were listed in Table 1. From Fig 2, all MnFe(x) hollow nanofibers with different Mn/Fe mole ratio showed typical IV curves and H1 type hysteresis loop, indicating that mesoporous structure come into being.[4,32] Upon increasing Mn doping content, the surface area improved from 96.5 to 137.1 m^2/g (Table 1), meanwhile higher manganese loading would enhance NO conversion until the mole ratio of $MnOx/Fe_2O_3$ reached 0.15. Beyond this value, a further increase of manganese loading could lead to sintering or the collapsing of the structure, which was harmful to the BET surface and catalytic activity. It is implied that the low-temperature reduction activity of NOx is related to the apparent surface properties to some extent. As shown in Table 1 and Fig. 6, both the BET surface (124.4 m^2/g) and the low temperature activity of MnFe(0.20) catalyst were lower than that of MnFe(0.15). This phenomenon is also verified by the scanning electron microscopic (SEM) images of these catalysts (Figure 3a-c).

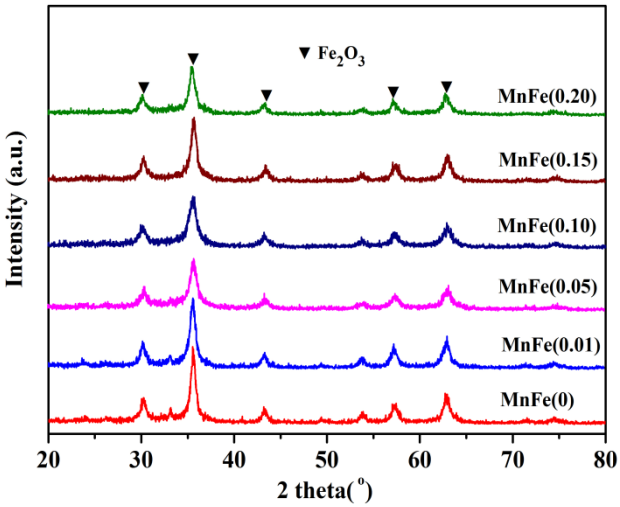

Fig. 1. XRD patterns of MnFe hollow nanofibers.

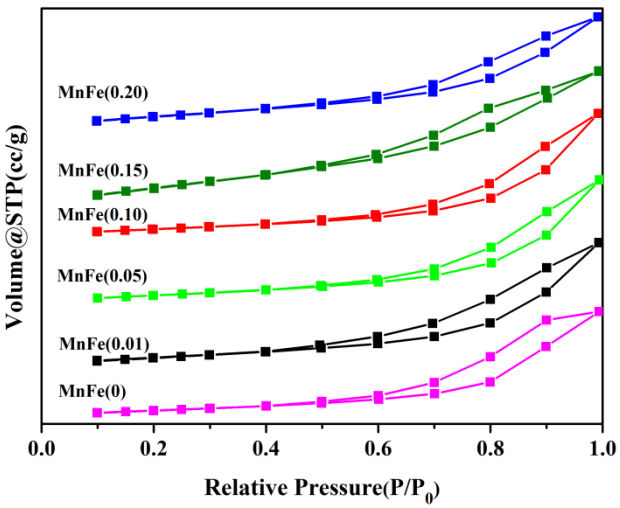

Fig. 2. Nitrogen adsorption isotherms of MnFe nanofibers

Table 1 The specific area, pore volume and pore diameter distribution of MnFe nanofibers

materials	specific area (m^2/g)	pore volume (cc/g)	pore diameter (nm)
Fe_2O_3	96.5	0.29	8.8
MnFe(0.01)	102.2	0.29	8.8
MnFe(0.05)	108.2	0.26	8.8
MnFe(0.10)	112.8	0.30	6.1
MnFe(0.15)	137.1	0.35	6.6
MnFe(0.20)	124.4	0.27	6.8

3.2 SEM and TEM analysis

Fig. 3 showed a typical scanning electron microscopy (SEM) and transmission electron microscopy (TEM) image of the as-prepared MnFe hollow nanofibers. From Fig. S1, it can be seen that the MnFe (0.05) nanofibers had hollow structure but non-uniform size. As to MnFe (0.20) (Fig. S2), the hollow structure is partially incomplete and collapsed, the result was consistent with the N_2 adsorption-desorption isotherms conclusion. As shown in Fig. 3c, all of MnFe (0.15) nanofibers were hollow structure and almost nanofibers were quite uniform in cross-section, and there were almost 60% of hollow nanofibers with outer diameter from 50 nm to 200 nm. The change of outer diameter should be attributed to the gradual loss of citrate agents from the nanofibres and the crystallisation of Fe_2O_3. After calcinations, the hollow MnFe(0.15) nanostructured fibers were smooth and composed of numerous nanoparticles with relatively uniform distribution of normally 5-20 μm long and have larger coarser surfaces, which provided a larger accessible surface area between the gas molecules and catalyst. Fig. 3b clearly indicated that the uniform tubular structure with an outer diameter 312 nm and 10 nm of wall thickness. TEM and HRTEM were also used to check the microstructure of catalyst MnFe (0.15). As shown in Fig. 3a, a typical hollow tubular structure with average outer diameter of about 140 nm and well-uniform wall thickness could be observed easily. Additionally, High-resolution transmission electron microscopy (HRTEM) was used to characterize the lattice structure. In addition, the two different lattice fringes can be clearly observed in Fig. 3d, one was around 0.361 nm, which matched with Fe_2O_3 (0.361 nm) in plane (011) and the other was 0.293 nm, corresponding to Fe_2O_3 (0.295 nm) in (110) or manganese oxides (0.291 nm) in (201).[20,33] These results indicate that the synthesized hollow fibers have good crystallinity and provide a large accessible surface area.

The possible formation mechanism of electropsun hollow nanofibers is the following: After electrospinning the xerogel nanofibers, a rigid outer shell came into being. However, it was still fluid in center of fibers that time, and a large amount of solvent and citric acid anions remained in the gel fibers. When the gel fiber was calcined in a tubular furnace, the sol particles diffused to the inner surface of the outer shell with the evaporation of the organic compounds, and thus the novel tubular structure first formed. Even at this stage, there were still many organic parts remaining in the fibers. Upon increasing the heating temperature, citrate anions began to decompose to produce CO_2 and H_2O gases, which went out of the fibers through the tube, and a crystallized hollow fiber produced.[34]

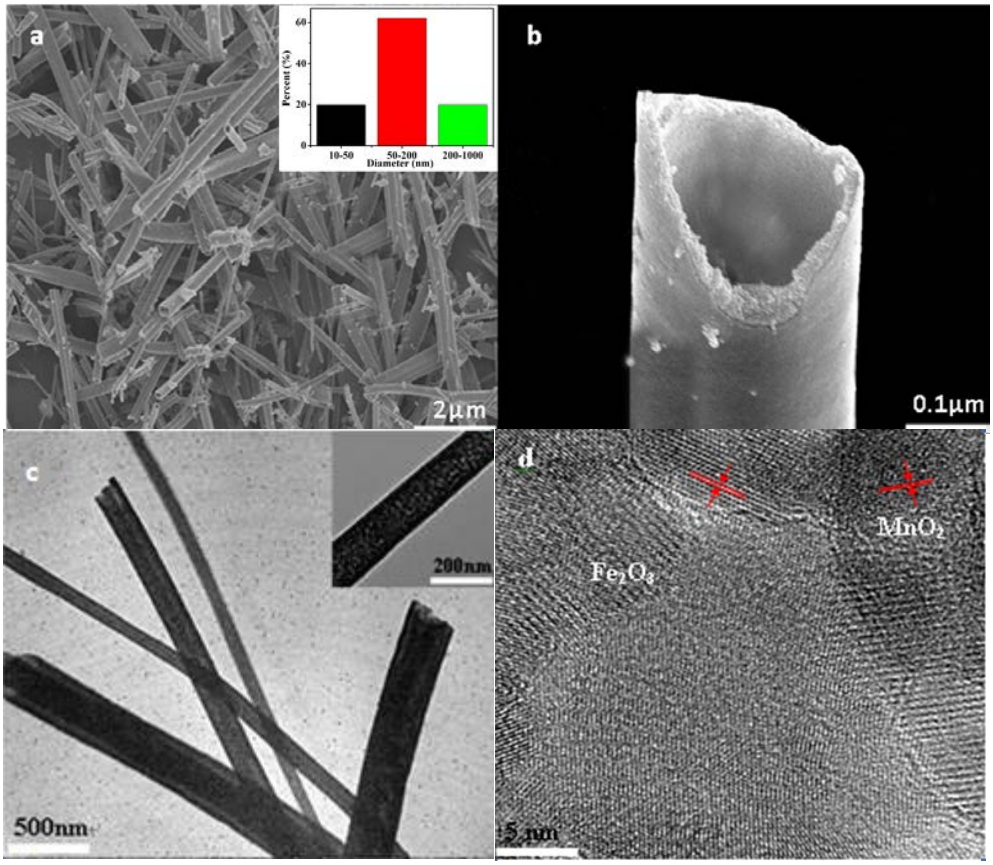

Fig. 3. (a) SEM image of electrospun MnFe (0.15) hollow nanofibers (inset: under high magnification); (b) SEM image of the cross-section; (c) TEM image of MnFe (0.15) hollow nanofibers; (d) HRTEM image of MnFe (0.15) hollow nanofibers.

4.1 H_2-TPR and XPS analysis

H_2-TPR is a widely used technique to investigate the redox properties of catalyst. The H_2-TPR profiles of Fe_2O_3, MnFe (0.05), and MnFe (0.15) catalyst were illustrated in Fig. 4. All H_2 consumption peaks could be attributed to the reduction of iron, manganese species, and their reduction behavior was very different. For the Fe_2O_3 sample, there were two peaks spanned over 250-550 °C and 600-800 °C, which was corresponding to the following reduction steps: Fe_2O_3-Fe_3O_4 (327°C) and Fe_3O_4-FeO (619°C), respectively. [35,36] It can be seen from this figure that the peak positions shifted to higher temperatures after the introduction of manganese. The peak from 300 °C to 400 °C can be ascribed to the combined reduction of Fe^{3+} and Mn^{3+} (or Mn^{4+}) with a structural transformation from $Fe_{2-y}Mn_yO_3$ to $(Fe\text{-}Mn)_3O_4$.[24,37] For these catalysts, there is likely to be a stronger metal-support interaction, thereby making it more difficult to carry out the reduction. For the MnFe (0.15) sample, increasing Mn loading decreases the temperature required for reduction of Fe_3O_4-FeO (662°C) compared to the MnFe (0.05) sample (705°C), it is suggested that the mobility of surface oxygen was enhanced after the addition of Mn, and therefore there was more chemisorbed oxygen formed on the catalyst surface.[38]

In order to understand the nature of the interaction between the two metal oxide species, the oxidation states of Fe $2p_{3/2}$, Mn $2p_{3/2}$, and O 1s in on MnFe hollow nanofibers were detected by XPS in Fig. 5, which had been calibrated against the C ls peak standardized at 284.6 eV. As shown in Fig. 5a, the Fe $2p_{3/2}$ peak is separated into two peaks by the same peak fitting deconvolution technique. The peaks at 711.0 and 713.1 eV can be assigned to Fe^{2+} and Fe^{3+}, respectively.[19] The ratios of Fe^{2+}/ Fe^{3+} on the surface of MnFe (0), MnFe (0.05) and MnFe (0.15) were approximately 0.80, 0.82 and 0.83, respectively, indicating that the increasing content of Mn increased the content of Fe^{2+}, which required higher reduction temperature than Fe^{3+}.

As shown in Fig. 5b, two main peaks due to Mn $2p_{3/2}$ and Mn $2p_{1/2}$ can be observed from 642.5 eV to 653.9 eV. By performing a peak-fitting deconvolution, the Mn $2p_{3/2}$ spectra were separated into three peaks, Mn^{3+} (641.5 – 641.8 eV), Mn^{4+} (642.7 – 643.1 eV) and Mn nitrate (644.8 – 645.2 eV).[39] It could be clearly seen that the intensities of Mn^{4+} characteristic peaks increased with the addition of Mn, accompanied with a decrease of Mn^{3+} peaks. The ratios of Mn^{4+}/ Mn^{3+} on the surface of MnFe (0.05) and MnFe (0.15) were approximately 1.2 and 2.5, respectively. Furthermore, the surface atom concentrations of Mn, Fe, and O and the atomic

ratios of Mn/Fe were summarized in Table 2, the percent of $O_{\square}$ on MnFe (0.15) fibers increased obviously with the increased Mn content. which were sure to increase the activity for NO oxidation to NO_2 and thereby enhance the "fast SCR" reaction activity ($4NH_3 + 2NO + 2NO_2 \rightarrow 4N_2 + 6H_2O$).[40] The O1s spectrum in Fig. 5c could be decomposed into two peaks, corresponding to various oxygen containing chemical bonds. According to the previous literature, the sub-bands at lower binding energy (530.0-530.4 eV) corresponded to the lattice oxygen (denoted as O_β), and the sub-bands at higher binding energy (532.2-532.5 eV) corresponded to the surface adsorbed oxygen (denoted as O_α), such as O_2^{2-} or O^- belonging to defect oxide or hydroxyl-like group.[22,41] As listed in Table 2, with the increasing of Mn doping, the chemisorbed oxygen O_α content was gradually increased, the ratios of $O_\alpha/(O_\alpha+O_\beta)$ over Fe_2O_3, MnFe (0.05) and MnFe (0.15) nanofiber were 18.4 %, 27.0% and 37.5%, respectively. It may be related to the presence of the Mn^{3+} species could create a charge imbalance, vacancies, and unsaturated chemical bonds on the catalyst surface, which would lead to the increase of oxide defects or hydroxyl-like groups. As we all know, surface chemisorbed oxygen was thought as the most active oxygen and played an important role in oxidation reactions. This meant that the MnFe (0.15) nanofibers might have better activity for the oxidation of NO to NO_2 than pure Fe_2O_3 in the NH_3-SCR process.

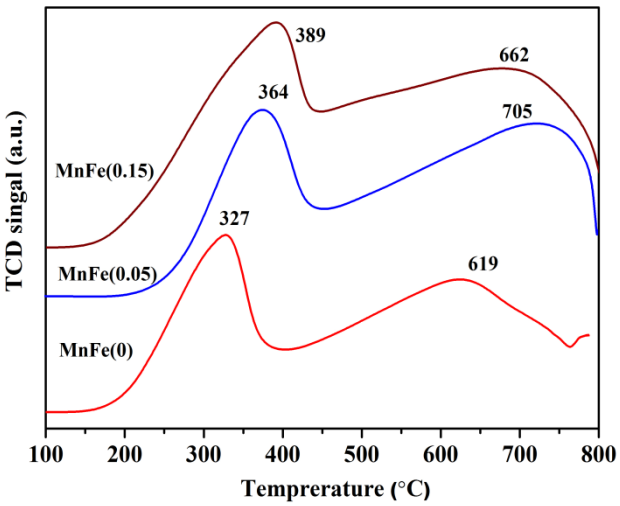

Fig. 4. H_2-TPR profiles of MnFe hollow nanofibers.

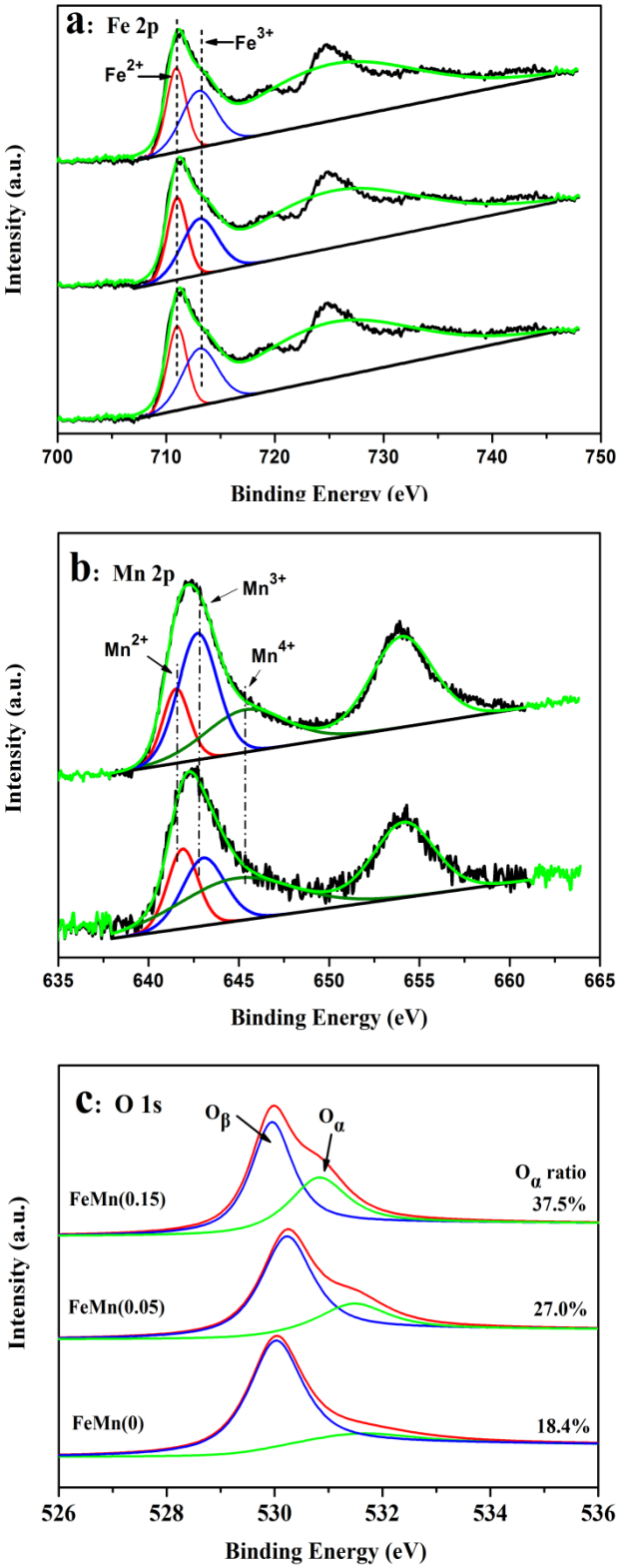

Fig. 5. (a) Fe 2p, (b) Mn 2p and (c) O1s from XPS spectra of MnFe nanofiber.

Table 2. XPS Results of Various Catalysts

Hollow fibers	Surface Atomic Concentration (%)				
	Fe	Mn	O_a	O_β	O_{total}
Fe_2O_3	29.3	0	13.01	57.69	70.7
MnFe (0.05)	24.41	2.48	19.74	53.37	73.11
MnFe (0.15)	17.95	6.47	28.34	47.74	75.58

3.3 Low-temperature catalytic performance

The NOx conversions, N_2 selectivities, and N_2O formations of the Mn-Fe catalysts with different molar ratios of Fe/Mn were shown in Fig. 6. Experimental results showed that there was only 38-80% NOx conversion when pure Fe_2O_3 was used as SCR catalyst at 100-300 °C, the addition of Mn content could significantly increase NOx conversion below 250 °C. It was found that the NOx conversion was greatly improved from 38 to 100% with an increase of Mn/ Fe molar ratio from 0 to 0.2 at 150 °C, the N_2 selectivity decreased with an increase of Mn/ Fe molar ratio (as shown in Fig. 6b). For the MnFe (0.15) catalyst, the NOx conversion was approximately 100% at 150 °C, and the amount of N_2O formed was below 20 ppm at 150 °C, indicating its promising N_2 selectivity.

The influences of 200 ppm SO_2 and 8 vol% H_2O on the performance of the MnFe (0.15) catalyst were investigated at 150 °C and the results were illustrated in Fig. 6c. It could be seen that a slight NO conversion decline occurred during 200 ppm SO_2 was added and then became stable, after removing SO_2 the conversion recovered to 92%. When 8 vol% H_2O was introduced into the stream, the NO conversion declined and kept at about 96%, after stopping H_2O the conversion restored to 99%. When the 200 ppm SO_2 and 8 vol% H_2O were injected into the feed gases at the same time, NO conversion decreased a little more, but the NO conversion still maintained at about 82%. The above results suggested that the catalyst had certain SO_2/H_2O durability.

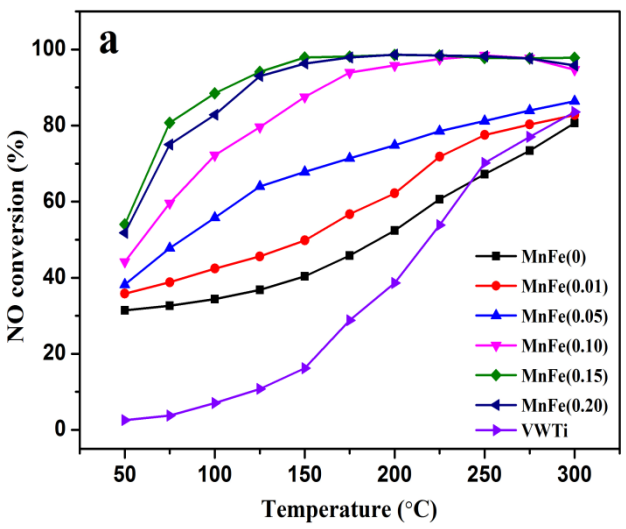

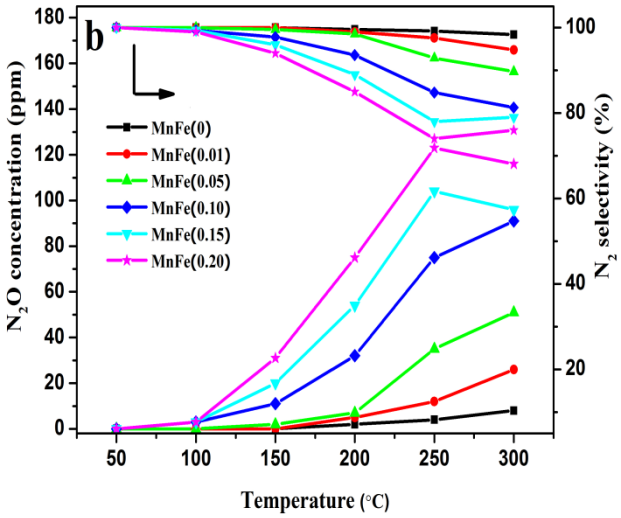

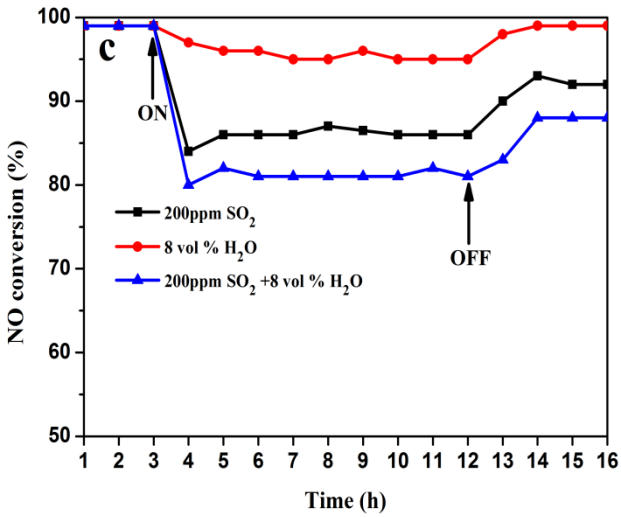

Fig. 6 (a) NOx conversion using MnFe (x) hollow fibrous catalyst and VWTi catalyst; (b) N_2 selectivity and N_2O concentration in the SCR reaction; (c) Influence of H_2O and SO_2 on NO conversion in the SCR reaction over MnFe (0.15) catalyst at 150 °C. Reaction conditions: [NO] = 500 ppm, [NH_3] = 500 ppm, [SO_2] = 200 ppm, [H_2O] = 8%, [O_2] = 5%, GHSV = 50,000 h^{-1}.

3.4 In situ FT-IR analysis

To investigate detailed reaction mechanism, the in situ DRIFTS experiment of reaction between NH_3 and pre-adsorbed NO + O_2 species at 150 °C was carried out and the results are shown in Fig. 7. In this experiment, the hollow nanofibers was first treated with NO+O_2 /Ar for 1 h and then purged with Ar for 30 min. When NH_3 was introduced at 150 °C, the DRIFT spectra could be recorded as a function of time (Fig. 7a). After NH_3 passed over the NO + O_2 pretreated catalyst, the band at 1610 cm^{-1} due to NO_2 [41] decreased and after 1min, the bidentate nitrate species (1580 cm^{-1})[30] on manganese oxides gradually disappear. After NH_3 was introduced for 10min, the band at 1580cm^{-1} disappeared, indicating that bidentate nitrate had participated in the reaction process, the band at 1550 cm^{-1} appeared, which could be assigned

to the intermediate of oxidation of ammonia.[42,43] As already noted, the intensity of the band at 1240 cm^{-1} due to bridged nitrate increases obviously, and its position shifted to 1260 cm^{-1}, which could be ascribed to the deformation nitrate species.[44] Meanwhile, the IR bands attributed to coordinated NH_3 (1260 and 1602 cm^{-1}) on the Lewis acid sites, ionic NH_4^+ (1440 cm^{-1}) on Brønsted-acid sites appeared, and the bands in the region of 3700-3000 cm^{-1} attributed to N-H stretching vibration could also observed.[45] After the catalyst was purged with NH_3 for 10 min, both adsorbed NH_3 and NO_x species could be observed on the catalyst surface. These results indicated that only the reaction between NO_2 and ammonia had occurred, not others. Furthermore, the coexistence of ammonia and nitrate adspecies showed that NH_3 and NO_x could be adsorbed over different active sites of catalyst surface.

In this experiment, the reactants were introduced to the MnFe(0.15) catalyst in the reversed order (as shown in Fig. 7b). After the MnFe(0.15) catalyst was first purged with NH_3 for 30 min, the catalyst surface was mainly covered by coordinated NH_3 (1207, 1230, 1440, 1602 and 1640 cm^{-1}).[45] When NO + O_2 was introduced for 2 min, the bands due to adsorbed NH_3 species decrease slightly and totally disappear after 10 min. At the same time, the nitrate species begin to form on the catalyst surface. However, bands at 1560 cm^{-1} increased a bit, which could also prove oxidation of ammonia such as nitrate or nitrite.[41] After the catalyst was purged with NO+O_2 for 20 min, the catalyst surface was mainly covered by monodentate nitrate (1365 cm^{-1} and 1560 cm^{-1}).[30,46] On the basis of the above results, it can be concluded that coordinate NH_3 played important roles in reducing NO_x in SCR reaction.

In general, when the SCR reaction happened at 150 °C, both adsorbed NH_3 and NOx species were considered to be involved in the SCR reaction. Besides, the coordinated NH_3 as well as in situ formed NO_2 species were considered to be involved in the NH_3–SCR reaction following an L-H mechanism.[47,48]

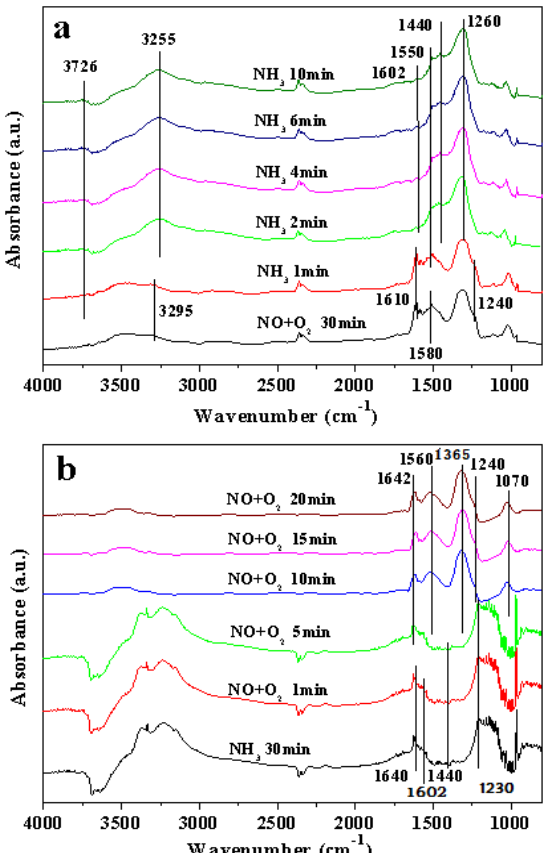

Fig. 7. In situ DRIFT spectra of MnFe (0.15) catalyst for the reaction between (a) NH_3 and adsorbed NOx at 150 °C, (b) NO + O_2 and adsorbed NH_3 species at 150 °C.

Conclusions

In this paper, hollow MnFe nanofibers with different Mn doping content were prepared by the electrospinning method, which were highly active for the low temperature selective catalytic reduction (SCR) of NO with NH_3. The MnFe(0.15) hollow fibers showed the highest activity and 100% NOx conversion at 150 °C with a space velocity of 50,000 h^{-1}. In addition, the large BET surface areas present in the catalyst also contributed to facilitate the SCR reaction. Based on in situ DFTIR analysis, more surface acidity, the formation of the intermediate, and the better low temperature reducibility properties, would be the main reasons for the high low-temperature catalytic activity.

Acknowledgements

The authors gratefully acknowledge the financial support of national natural foundation of china (21377061), Asia Research Center in Nankai University (AS1326), Natural Science Foundation of Tianjin (12JCQNJC05800), Key Technologies R&D Program of Tianjin (13ZCZDSF00300) and the assistance of Dr. Raymond Seekell (University of Notre Dame) in manuscript preparation and discussion.

Notes and references

[a] *College of Environmental Science and Engineering, Key Laboratory of Environmental Pollution Process and Environmental Criteria, Nankai*

University, Tianjin 300071, P. R. China; E-mail: sihuizhan@nankai.edu.cn or jkcs66902@163.com, Tel/Fax: +86-22-23502756.
[b] *Department of Chemistry, Tianjin University, Tianjin 300072, P. R. China, E-mail: liyi@tju.edu.cn*

1 K. Mathisen, D.G. Nicholson and A.N. Fitch, J. Mater. Chem., 2005, **1**, 204-217.
2 R. M. Tost, J.S. Gonzalez and P. M. Torres, J. Mater. Chem., 2002,**11**, 3331-3336.
3 Z.B. Wu, B.Q. Jiang, Y. Liu, W.R. Zhao and B.H. Guan, J. Hazard. Mater., 2007, **145**, 488-494.
4 C.C. Zhou, Y.P. Zhang, X.L. Wang, H.T. Xu, K.Q. Sun and K. Shen, J. Colloid. Interface. Sci., 2013, **392**, 319-324.
5 E. James, II. Parks, Science., 2010, **26**, 1584-1585.
6 X.Y. Shi, F.D. Liu, L.J. Xie, W.P. Shan and H. He, Environ. Sci. Technol., 2013, **47**, 3293-3298.
7 Y. Li, J.H. Peng, X. Huang, X. Li, W.K. Su, X.X. Sun, D.Z. Wang and J.M. Hao, Environ. Sci. Technol., 2014, **48**, 4515-4520.
8 Q. Li, H.S. Yang, F.M. Qiu and X.B. Zhang, J. Hazard. Mater., 2011, **192**, 915-921.
9 J. Li, H. Chang, L. Ma, J. Hao and R.T. Yang, Catal. Today., 2011, **175**, 147-156.
10 M.S. Maqbool, A.K. Pullura and H. P. Ha, Appl. Catal. B., 2014, **152-153**, 28-37.
11 Y. Peng, J. Li, W. Shi, J. Xu and J. Hao, Environ. Sci. Technol., 2012, **46**, 12623-12629.
12 R.H. Gao, D.S. Zhang, X.G. Liu and L.Y. Shi, Catal. Sci. Technol., 2013, **1**, 191-199.
13 F.D. Liu, H. He, C.B. Zhang, W.P. Shan and X.Y. Shi, Catal. Today., 2011, **175**, 18-25.
14 L. Chen, J.H. L and M.F. Ge, Chem. Engineer. J., 2011, **170**, 531-537.
15 J. Chen, M. Shen, X. Wang, G. Qi, J. Wang, W. Li., Appl. Catal., 2013, **134-135**, 251-257.
16 P. Fabrizioli, T. Burgi and A. Baiker, J. Catal., 2002, **206**, 143-154.
17 M.A. Larrubia, G. Ramis and G. Busca, Appl. Catal. B: Environ., 2001, **30**, 101-110.
18 Y.J. Kim, H.J. Kwon, I.S. Nama, J.W. Choung, J.K. Kil, H.J. Kim, M.S. Cha and G.K. Yeo, Catal. Today., 2010, **151**, 244-250.
19 S. Roy, B. Viswanath, M.S. Hegde and G. Madras, J. Phys. Chem. C., 2008, **112**, 6002-6012.
20 Z.L. Liu, Y. Yi, S.X. Zhang, T.L. Zhu, J.Z. Zhu and J.G. Wang, Catal. Today., 2013, **216**, 76-81.
21 W. Tian, H. Yang, X. Fan and X. Zhang, J. Hazard. Mater., 2011, **188**, 105-109.
22 Z. Chen, F. Wang, H. Li, Q. Yang, L. Wang and X. Li, Ind. Engin. Chem. Res., 2012, **51**, 202-212.
23 H. Li, D. Zhang, P. Maitarad, L. Shi, R. Gao, J. Zhang and W. Cao, Chem. Commun., 2012, **48**, 10645-10647.
24 J. Shan, Y. Zhu, S. Zhang, T. Zhu, S. Rouvimov and F. Tao, J. Phys. Chem. C., 2013, **117**, 8329-8335.
25 S. Yang, J. Li, C. Wang, J. Chen, L. Ma, H. Chang, L. Chen, Y. Peng and N. Yan, Appl. Catal. B: Environ., 2012, **117-118**, 73-80.
26 H.Q. He, J. Yin, Y.X. Li, Y. Zhang, H.S. Qiu and J.B. Xu, Appl. Catal. B: Environ., 2014, **156-157**, 35-43.
27 S. Kim, S.K. Lim, Appl. Catal. B: Environ., 2008, **84**, 16-20.
28 C. Wessel, R. Ostermann, R. Dersch and B.M. Smarsly, J. Phys. Chem. C., 2011, **115**, 362-372.
29 D. Ma, Y.J. Xin, M.C. Gao and J. Wu, Appl. Catal. B: Environ., 2014, **147**, 49-57.
30 S.J. Yang, C.Z. Wang, J.H. Li, N.Q. Yan, L. Ma and H.Z. Chang, Appl. Catal. B: Environ., 2011, **110**, 71-80.
31 X.C. Li, V.T. John, J.J. Zhan, G.H. He, J.B. He and L. Spinu, Langmuir., 2011, **27**, 6252-6259.
32 Y. Wan, W. Zhao, Y. Tang, L. Li, H. Wang, Y. Cui, J. Gu, Y. Li and J. Shi, Appl. Catal. B: Environ., 2014, **148–149**, 114–122.
33 C.R. Gong, D.R. Chen, X.L. Jiao and Q.L. Wang, J. Mater. Chem., 2002, **12**, 1844-1847.
34 S.H. Zhan, J.Y. Yang, Y. Liu, N. Wang, J.J. Dai, H.B. Yu, X.C. Gao and Y. Li, J. Colloid. Interface. Sci., 2011, **355**, 328-333.
35 G. Giecko, T. Borowiecki, W. Gac and J. Kruk, Catal. Today., 2008, **137**, 403-409.
36 M.R. Morales, B.P. Barbero and L.E. Cadus, Appl. Catal. B: Environ., 2007, **74**, 1-10.
37 C. Wang, S. Yang, H. Chang, Y. Peng and J. Li, J.Mol. Catal. A: Chem., 2013, **376**, 13-21.
38 B. Thirupathi, P.G. Smirniotis, J. Catal., 2012, **288**, 74-83.
39 D.A. Peña, B.S. Uphade and P.G. Smirniotis. J. Catal., 2004, **221**, 421-431.
40 Y.J. Kim, H.J. Kwon, I. Heo, I.S.Nam, B.K.Cho, J.W. Choung, M.S. Cha and G.K. Yeo, Appl. Catal. B., 2012, **126**, 9-21.
41 Y. Shu, H. Sun, X. Quan and S. Chen, J. Phys. Chem. C., 2012, **116**, 25319-25327.
42 L. Chen, J. Li and M. Ge., Environ. Sci. Technol. 2010, **44**, 9590-9596.
43 Y. Shu, H. Sun, X. Quan and S. Chen., J. Phys. Chem. C., 2012, **116**, 25319−25327.
44 M. Casapu, O. Krocher, M. Mehring, M. Nachtegaal, C. Borca, M. Harfouche and D. Grolimund, J. Phys. Chem. C., 2010, **114**, 9791-9801.
45 G. Ramis, M.A. Larrubia, J. Mol. Catal. A. 2004, **215**, 161-167.
46 A. Karami, V. Salehi, J. Catal., 2012, **292**, 32-43.
47 H.J. Chae, S.T. Choo, H. Choi and I.S. Nam, Ind. Eng. Chem. Res., 2000, **39**, 1159-1170.
48 A. Shi, X. Wang, T. Yua and M. Shen. Appl. Catal., 2011, 106, 359-369.

Table of Contents

Facile preparation of MnO_2 doped Fe_2O_3 hollow nanofibers for low temperature SCR of NO with NH_3

Sihui Zhan,*[a] Mingying Qiu, *[a] Shanshan Yang[a], Dandan Zhu,[a] Hongbing Yu [a] and Yi Li*[b]

[a] *College of Environmental Science and Engineering, Key Laboratory of Environmental Pollution Process and Environmental Criteria, Nankai University, Tianjin 300071, P. R. China; E-mail: sihuizhan@nankai.edu.cn, Tel/Fax: +86-22-23502756.*

[b] *Department of Chemistry, Tianjin University, Tianjin 300072, P. R. China, E-mail: liyi@tju.edu.cn*

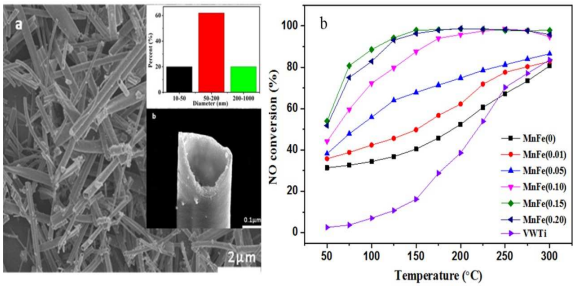

MnO_2 doped Fe_2O_3 hollow nanofibers were successfully synthesized by electrospinning method, which exhibit superior catalytic activity for low temperature NH_3-SCR.